High-pressure compressibility and electronic properties of bismuth silicate Bi_2SiO_5 from synchrotron experiments and first-principles calculations

A. Girard,[1,*] M. Stekiel,[1] W. Morgenroth,[1] H. Taniguchi,[2] V. Milman,[3] A. Bosak,[4] and B. Winkler[1]

[1]*Institut für Geowissenschaften, Goethe Universität Frankfurt, Altenhöferallee 1, D-60438 Frankfurt am Main, Germany*

[2]*Department of Physics, Nagoya University, Nagoya 464-8602, Japan*

[3]*Dassault Systèmes BIOVIA, CB4 0WN Cambridge, United Kingdom*

[4]*ESRF - The European Synchrotron, 71, Avenue des Martyrs, F-38000 Grenoble, France*

(Received 26 November 2018; revised manuscript received 5 February 2019; published 28 February 2019)

The high-pressure structural properties of bismuth oxide Bi_2SiO_5 have been investigated up to 29 GPa using *in situ* powder synchrotron x-ray diffraction (XRD) and up to 50 GPa with density functional theory (DFT) calculations. We found a compressibility anomaly at about 20 GPa that is observed both in our XRD and DFT results. The rotation of the corner-connected SiO_4 tetrahedra produces a straightening of the silicate chains, yielding a lower compressibility above 20 GPa for the structure with straight chains. We analyzed the stereochemical activity of the Bi^{3+} lone electron pair, which is found to decrease with increasing pressure, but it can still be identified in the calculated electron density difference maps at 50 GPa.

DOI: 10.1103/PhysRevB.99.064116

I. INTRODUCTION

Currently, there is a considerable interest in ferroelectric lead-free oxide materials with high transition temperatures. In this context, Bi_2SiO_5 (BSO) has emerged as a promising lead-free oxide, after the finding of high-temperature ferroelectricity with a transition from the *Cc* to the *Cmcm* phase at the Curie temperature $T_C = 670$ K [1,2]. Apart from ferroelectricity, another interesting electronic feature in BSO is the lone electron pair located at the irregularly coordinated Bi atom. In contrast to other lone-pair-electron-driven displacive-type ferroelectrics [3] or multi- and ferroelectric compounds with perovskite-type structures, where the spontaneous polarization arises from the cation off-centering ($BiFeO_3$ [4], $BiMnO_3$ [5], $PbTiO_3$), the ferroelectricity in BSO is primarily driven by the tilt of the SiO_4 units [6] within the one-dimensional (1D) tetrahedral chains, characteristic for this structure. These findings have triggered numerous experimental and theoretical studies, making BSO a benchmark system for ferroelectrics based on polymerized tetrahedra as an alternative to perovskite-type ferroelectrics.

At ambient conditions BSO is stable in the monoclinic *Cc* space group (see the structure in Fig. 1). A very small monoclinic distortion of the crystallographic angle β from 90° to 90.0695° was reported based on transmission electron microscopy measurements and Rietveld refinements [1]. Characteristic for the BSO structure at ambient conditions are chains of corner-sharing SiO_4 tetrahedra aligned along the *c* axis. These chains are located in layers parallel to the (b, c) plane. Bi atoms are also located on planes parallel to the (b, c) plane, and are irregularly coordinated by six oxygens located on one side of the Bi atom, while the lone electron pair is located at the other side. Based on *ab initio* calculations, Park *et al.* [6] concluded that the spontaneous polarization along the *c* axis was overwhelmingly due to tetrahedral tilting. A systematic tuning of the ferroelectric phase transition is possible by element substitution, where Pb was successfully substituted for Bi up to 20% [7].

Besides the importance of BSO as a benchmark system to design new tetrahedra-based ferroelectrics, this compound is also interesting as a model system to study the interplay between ferroelectric and antiferroelectric ordering. It was observed by Taniguchi *et al.* that the ferroelectric-paraelectric phase transition at T_C is driven by the freezing of an optical phonon at the Γ point [1], as is usually observed in ferroelectric materials [8]. However, in a recent study an additional dynamical anomaly at the Brillouin zone edge was reported [9], where the *Y* point optical phonon substantially softens down to ∼50% when approaching the T_C. The phonon softening was observed along the whole Γ-*Y* optical branch, presumably producing a collapse of the transverse acoustic branch due to transverse optical (TO)-transverse acoustic (TA) mode coupling. Because the *Y* point phonon is intrinsically associated with antiferroelectric displacements, the simultaneous observation of a zone center and a zone boundary dynamical anomaly is evidence for a competition between ferroelectric and antiferroelectric ordering in BSO [9]. The outcome of such competition can strongly depend on an external perturbation, such as pressure. However, the pressure dependence of BSO has not been reported yet, which was the main motivation for carrying out the present study.

In this paper we report a high-pressure structural study of BSO based on *in situ* powder diffraction synchrotron experiments and density functional theory (DFT) calculations. We address the activity of the stereochemically active lone electron pair on the Bi^{3+} ion under pressure and the compression mechanisms of the ferroelectric structure with an emphasis on the evolution of the 1D tetrahedral chains responsible for the ferroelectric properties of BSO.

*Corresponding author: adrien.girard@sorbonne-universite.fr

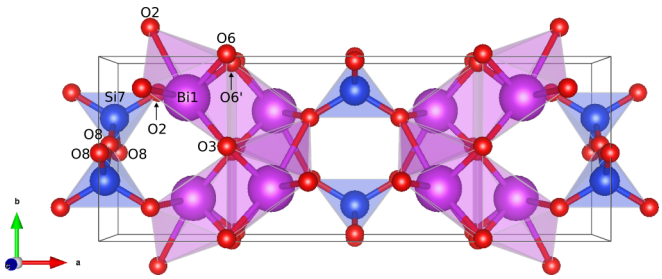

FIG. 1. Polyhedral representation of the unit cell of BSO at ambient pressure conditions. The blue, red, and violet spheres represent Si, O, and Bi atoms, respectively. The blue and violet polyhedra indicate the SiO_4 and BiO_6 coordination polyhedra. The silicate 1D chains are oriented along the c axis.

II. EXPERIMENT

Bi_2O_3 and SiO_2 powders were mixed in an agate mortar in a stoichiometric ratio and heated in a Pt crucible at 1373 K over 2 h. The resulting polycrystalline melt was subsequently cooled to ambient temperature and crushed to obtain fine powders.

High-pressure diffraction data were recorded at the Extreme Conditions Beamline P02.2 at PETRA III, Hamburg, Germany. The beam was focused to a spot size of 8×2.4 μm [full width at half maximum (FWHM), $H \times V$] using compound refractive lenses. The incoming photon energy was 42.66 keV (corresponding to 0.290 63 Å) and the detector to sample distance was 400 mm.

The BSO powder was loaded into the symmetric-type diamond-anvil cell (DAC) with 300-μm culet size diamonds. A rhenium plate preindented to 35-μm thickness was used as the gasket, in which a 150-μm-diam hole was drilled with an excimer laser. Au was used as the pressure marker [10] and neon was employed as a pressure-transmitting medium.

The pressure was increased in steps of 1–2 GPa. Before commencing with the data collection we waited for pressure equilibration. We collected data at two positions at each pressure. The maximum pressure achieved was 29 GPa. Data collection was performed in the oscillation mode (10° rotation in 10 s) to increase the number of crystallites in the diffraction condition. The two-dimensional x-ray diffraction (XRD) images were converted to a one-dimensional diffraction pattern using the DIOPTAS program [11]. For data analysis, Le Bail and Rietveld refinements were carried out with the JANA2006 software [12]. Additional ambient pressure data were recorded at the ID28 beamline side station [13] from the European Synchrotron Radiation Facility (ESRF) with a wavelength $\lambda = 0.5226$ Å.

III. COMPUTATIONAL DETAILS

First-principles calculations were carried out within the framework of density functional theory (DFT) [14], the Perdew-Burke-Ernzerhof (PBE) exchange correlation functional [15], and the plane-wave/pseudopotential method using the CASTEP [16] simulation package. "On the fly" norm-conserving pseudopotentials from the CASTEP database were employed in conjunction with plane waves up to a kinetic energy cutoff of 800 eV. A Monkhorst-Pack grid was used for Brillouin zone integrations with a distance of <0.023 Å^{-1} between the grid points. Convergence criteria included an energy change of $<5 \times 10^{-6}$ eV/atom for self-consistent-field (SCF) cycles, a maximal force of <0.008 eV/Å, and a maximal component of the stress tensor <0.02 GPa.

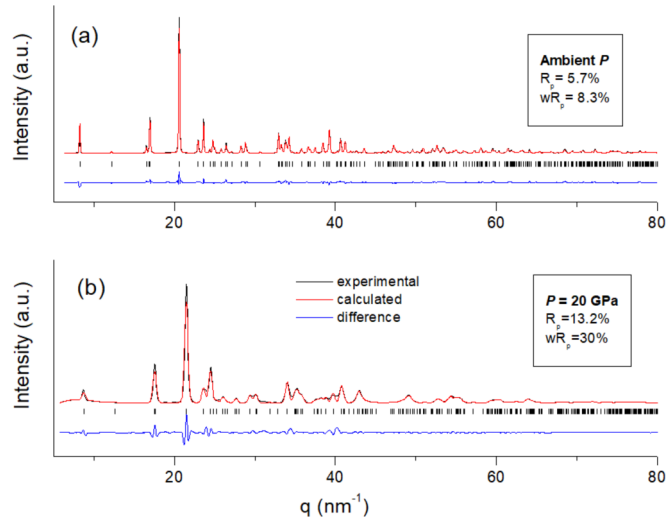

FIG. 2. (a) Examples of Le Bail refinements in the monoclinic structure at ambient pressure and (b) at high pressure at $P = 20$ GPa. R_p and wR_p factors are the result of the Le Bail fits.

IV. RESULTS AND DISCUSSION

A selection of powder diffraction patterns measured at ambient pressure in a capillary and under pressure at $P = 20$ GPa is shown in Figs. 2(a) and 2(b), respectively. Due to the presence of the strongly scattering Bi atoms, the extraction of reliable positional parameters for the much lighter elements was not possible for the data collected in a DAC. Hence, the analysis was restricted to a removal of the background and a subsequent Le Bail fit, from which the pressure dependence of the lattice parameters was obtained. The calculated diffractograms obtained with the Le Bail fitting procedure in the Cc space group are shown in Fig. 2, and the pressure-induced changes of the normalized lattice parameters are shown in Fig. 3(a) (see Supplemental Material for tabulated values [17]). The compression of the structure up to 29 GPa is only very slightly anisotropic, with a stronger compressibility of the long a axis, while the b and c axes show a similar variation with pressure. Above $P \sim 20$ GPa, we observe an anomaly in the compressibility, which became more obvious by looking at the lattice parameter ratios in Fig. 2(c). The ratios b/a and c/a have a very similar behavior, slightly increasing up to ~29 GPa, while the ratio c/b ratio smoothly changes towards another compressibility regime. Calculations show that these compressibility changes are related to the conformational changes of the chains of Si tetrahedrons in the (b, c) plane and will be discussed in more detail below. The P-V data for the low-pressure phase of BSO were fitted with a third-order Birch-Murnaghan equation of state (EOS) [18] from ambient pressure up to 17 GPa [see Fig. 3(b)]. The fit to the experimental P-V data lead to $V_0 = 444.3$ Å^3 (fixed),

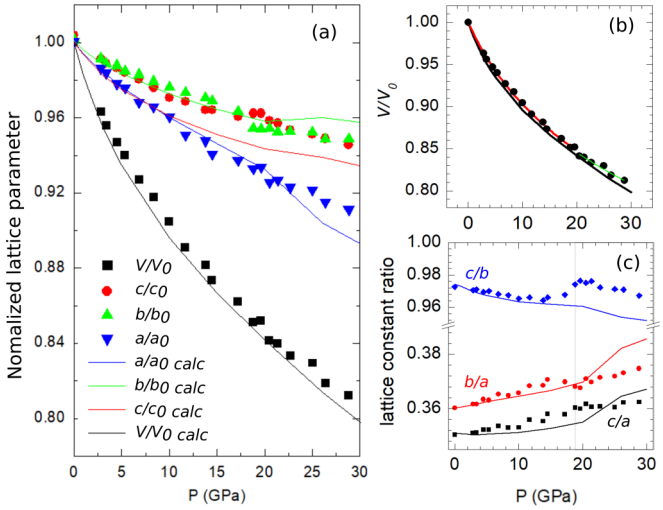

FIG. 3. (a) Pressure dependence of the normalized unit cell parameters. Solid symbols represent experimental data, and solid lines the results of DFT calculations. The subscript 0 refers to ambient pressure data. (b) Fit of an equation of state to the experimental data (black circles) for $P < 17$ GPa (red) and $P > 20$ GPa (green). The solid black line is the theoretical data for comparison. Resulting bulk moduli are summarized in Table I. (c) Evolution of the lattice parameter ratios with pressure. Solid symbols are experimental data, and solid lines are calculated data obtained from DFT.

$B_0 = 69(6)$ GPa, and $B_0' = 7(1)$, where B_0 is the bulk modulus, B_0' its pressure derivative, and V_0 the volume of the unit cell at ambient conditions (Table I). The fit parameters of the equation of state, namely, B_0 and B_0', are highly correlated, and to facilitate a comparison with other data we plotted confidence ellipses (see Supplemental Material).

We now turn to our theoretical results. The pressure dependence of the normalized lattice parameters and their ratios are plotted alongside with the experimental data in Fig. 3. Our experimental and calculated lattice parameters at ambient pressure are in reasonable agreement (∼2%, see Table II) with each other and earlier data. The ambient pressure DFT data deviate in one respect from the structural data published by Taniguchi *et al.* [1]. In our calculations, the Si-O distances of oxygens coordinating the Bi atoms are about 1.62 Å, i.e., a value typical for Si-O bonds in tetrahedra. However, the Si-O distances to those oxygen which are corner shared with the adjacent tetrahedra are unusually long (1.68 Å). At ambient pressure the Si-O-Si and O-Si-O angles in the

TABLE I. Bulk modulus B_0 (GPa) and its pressure derivative B_0' derived from fits of the experimental and theoretical P-V data ($P < 17$ GPa and $P > 20$ GPa) using a third-order Birch-Murnaghan equation of state, and derived from stress-strain calculations of the elastic stiffness tensor.

	B_0 (GPa)	B_0'	V_0 (Å^3)
Experiment ($P < 17$ GPa)	69 (6)	7 (1)	444.3
Experiment ($P > 20$ GPa)	73 (10)	7 (3)	444.3
DFT from EOS ($P < 17$ GPa)	58 (11)	9(3)	466
DFT from EOS ($P > 20$ GPa)	77 (9)	5 (1)	466
DFT from c_{ij}	55.6(7)		

TABLE II. Comparison of BSO unit cell parameters obtained from DFT calculations, from Le Bail refinement (this work), and from an earlier study [1].

	Expt. This study	DFT This study	Expt. [1]
a (Å)	15.195(1)	15.456	15.1193(1)
b (Å)	5.468(2)	5.5632	5.4435(1)
c (Å)	5.315(1)	5.4208	5.2892(1)
β (deg)	90.0	89.995	90.0695(20)

experimentally determined and computed structure are in very good agreement. A bond population analysis strongly supports the preference for a description of the Bi atom in sixfold coordination, instead of an alternative description where the Bi atom is the apex of a pyramid, as there still is an appreciable bond population of about 0.1 eV/Å^3 even for the longest [d_{max}(Bi-O) ≈ 2.59 Å] Bi-O distances. The irregular coordination polyhedron is, however, indicative for a stereochemical lone electron pair (see below).

The pressure dependence of the lattice parameters obtained from the DFT calculations shows a similar continuous change toward a secondary compressibility regime as that observed experimentally around 20 GPa, although the effect is slightly more pronounced in the calculations compared to our observations. The fit of an equation of state to the theoretical data gave $B_0 = 58(11)$ GPa, $B_0' = 9(3)$, and $V_0 = 466$ Å^3 (fixed)—see Table I (the fit was carried out for $P < 17$ GPa and $P > 20$ GPa separately). In order to independently assess the bulk modulus, we carried out stress-strain calculations for the derivation of the complete elastic stiffness tensor. We obtained the following values in GPa: $c_{11} = 108(2)$, $c_{22} = 122(2)$, $c_{33} = 131(1)$, $c_{44} = 42(1)$, $c_{55} = 42.2(5)$, $c_{66} = 48.0(4)$, $c_{12} = 45(2)$, $c_{13} = 10(2)$, $c_{23} = 16(2)$, resulting in a bulk modulus $B_0 = 55.6(7)$ GPa. All other tensor components which are allowed to differ from zero in the monoclinic system (c_{14}, c_{15}, c_{35}, c_{46}) were zero within the numerical uncertainty.

The DFT calculations allow us to follow in detail the mechanism responsible for this compressibility change at high pressure. The pressure dependences of the Si-O and Bi-O bonds are shown in Fig. 4. As has been noted above, the DFT calculations predict that at ambient conditions there are two bonds with the typical Si-O bond length of 1.62 Å, and two bonds which are slightly longer (1.68 Å). At 50 GPa, the bond lengths have decreased substantially to 1.55 and 1.60 Å, respectively. This prediction is in good agreement with experimental findings in other silicates. For example, a single-crystal high-pressure diffraction study of a silicate garnet $Bi_2Ga_4O_9$ gave a Si-O bond length of 1.58 Å at 50 GPa [19]. The coordination polyhedron around the Bi becomes less distorted on increasing pressure. At 50 GPa there are eight oxygen atoms within 2.8 Å of a Bi atom, but a population analysis indicates that along all these distances the population is very low (<0.08 e^-/Å^3 even for the shortest Bi-O distance), and hence there is no well-defined coordination polyhedron around Bi.

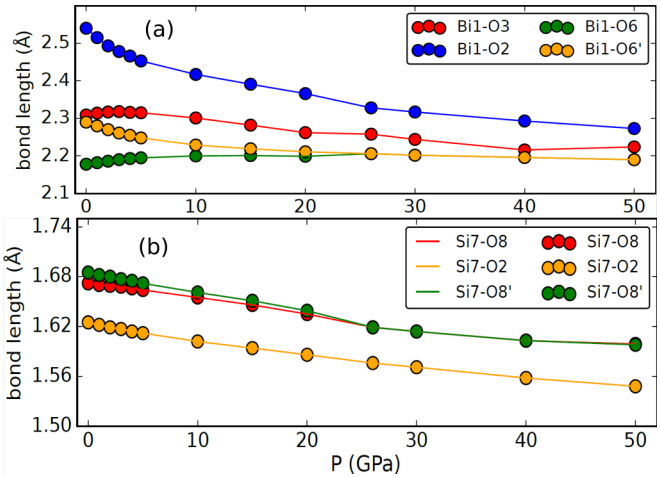

FIG. 4. Pressure dependence of the (a) Bi-O and (b) Si-O (b) bond lengths from DFT calculations, which predict that on pressure increase the bismuth coordination polyhedra become less distorted, while in the Si-O tetrahedra two longer and two shorter bonds are preserved up to 50 GPa.

The most striking effect is the evolution of the SiO_4 tetrahedral chains aligned along the c axis. The pressure-induced change of the O-O-O angle formed by the corner-sharing oxygen atoms along the chain, and the Si-Si distances are shown in Fig. 5. With increasing pressure, the chains shorten,

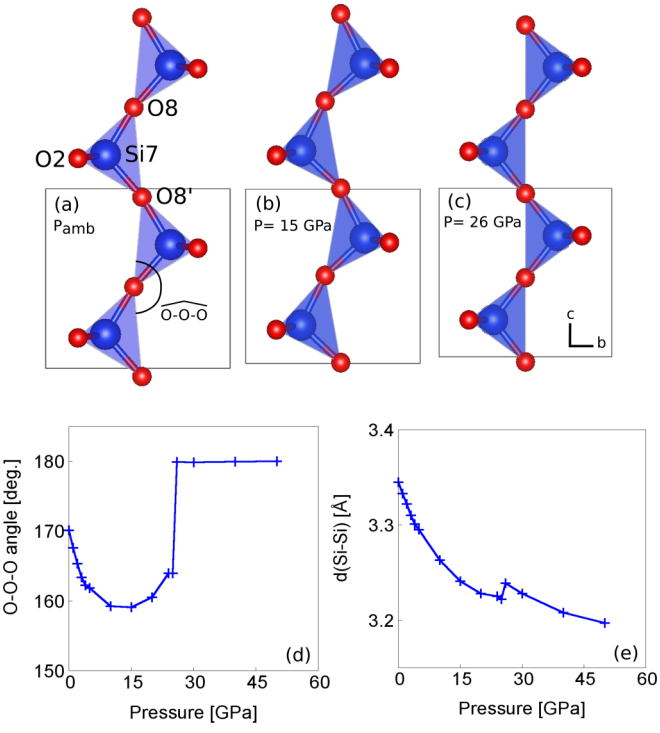

FIG. 5. (a)–(c) Evolution with pressure of the tilted tetrahedral chains aligned parallel to the [001] direction in the (b, c) plane as obtained from DFT. Only the silicate chains are displayed for clarity. (d) and (e) Evolution with pressure of the O-O-O angle and the Si-Si distance, respectively, showing the discontinuity at the phase transition.

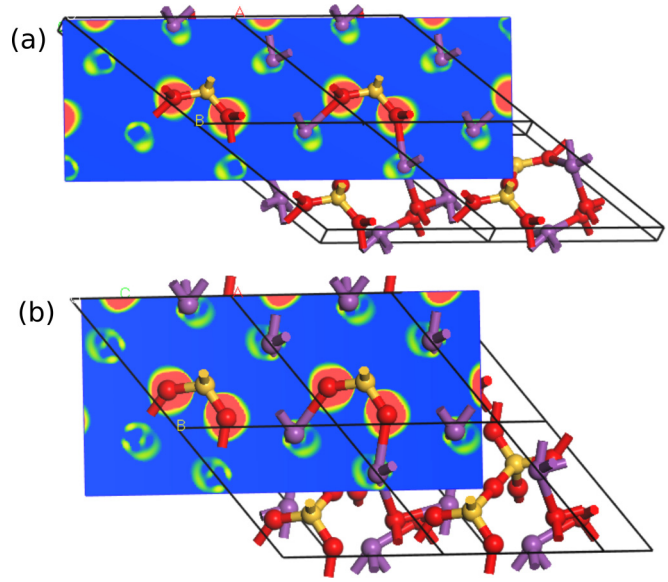

FIG. 6. Slice through the calculated valence electron density difference function of BSO at (a) ambient pressure and (b) 50 GPa. The maxima of the density difference function with a value of $\approx 0.04\, e^-/\text{Å}^3$ close to the Bi atoms are typical of stereochemically active lone electron pairs. While the maxima decrease with increasing pressure, they are still discernible at 50 GPa.

i.e., the Si-Si distances decrease through an increase of the tetrahedral tilt in the SiO_4 chains. This compression mechanism is similar as observed for quartz, the archetypal SiO_4-tetrahedral material [20]. Above 20 GPa, a rotation of the SiO_4 units leads to straight SiO_4 chains. The compressibility of the chain along the chain axis is significantly smaller for the straight chain than for the tilted chain, which is in line with the evolution of the lattice parameters (Fig. 3).

We also studied the effect of pressure on the Bi^{3+} $6s^2$ lone electron pair. We have evaluated the valence electron density difference function, i.e., the difference between the overlapping noninteracting atomic valence electron densities and the self-consistent electron density up to 50 GPa (Fig. 6). The calculations show clear evidence for a localized stereochemically active lone electron pair at low pressures, with a maximum density of $\approx 0.04\, e^-/\text{Å}^3$ close to the Bi atoms. At 50 GPa, this maximum is smeared out, but can still be detected, and hence the lone electron pair is still stereochemically active. The persistence of stereochemical lone electron pairs at high pressures has been observed in a range of other compounds, including PbO up to 46 GPa [21], $Bi_2Ga_4O_9$ [22] up to 50 GPa, and Bi_2S_3 [23,24]. In some other cases, the disappearance of the lone pair was observed [25].

The unexpected straightening of the SiO_4 octahedra at high pressures might have a very interesting influence on the ferroelectricity. As shown by Park *et al.* [6] at ambient conditions, the ferroelectricity of BSO arises mainly from the tilting of the SiO_4 chains forming the SiO_3 layer, 24.1 $\mu C/cm^2$, however, a small component originates from the Bi_2O_2 layer, 1.3 $\mu C/cm^2$. They have also shown that the spontaneous polarization is proportional to the tilting angle, which they defined as an angle complementary to the O-O-O

angle defined in this study. This allows us to predict that spontaneous polarization of BSO would increase with pressure, reaching a maximum at ∼15 GPa, and vanish at ≈20 GPa with the straightening of the silicate chains reminiscent of the ferroelectric-paraelectric transition [1].

V. CONCLUSIONS

In summary, we have performed a high-pressure study of the structure of BSO by synchrotron x-ray powder diffraction and DFT calculations. The compression mechanism of the *Cc* structure below 20 GPa is characterized by a continuous rotation of the SiO_4 tetrahedra, which leads to a shortening of the Si-Si distances and of the chain length. Above 20 GPa we observed a secondary compressibility regime, which could be explained by our DFT calculations: the continuous rotation of the SiO_4 tetrahedra leads to a straightening of the Si tetrahedral chains, with a lower compressibility of the structure with straight chains. Finally, the stereochemical activity of the Bi lone electron pair was found to persist and remain localized up to at least 50 GPa.

ACKNOWLEDGMENTS

This study was supported by the BMBF Projects No. 05K16RF1, No. 05K16RF2, No. 05K16RFA, and No. 05K16RFB, and a joint DFG-ANR Project No.WI1232/41-1. We acknowledge DESY (Hamburg, Germany), a member of the Helmholtz Association HGF, for the provision of experimental facilities. Parts of this research were carried out at PETRA-III and we would like to thank the P02.2 beamline staff for technical support. This work is partially supported by a Grant-in-Aid for Young Scientists (A) (No. 16H06115) and MEXT Element Strategy Initiative Project.

[1] H. Taniguchi, A. Kuwabara, J. Kim, Y. Kim, H. Moriwake, S. Kim, T. Hoshiyama, T. Koyama, S. Mori, M. Takata, H. Hosono, Y. Inaguma, and M. Itoh, Angew. Chem., Int. Ed. Engl. **52**, 8088 (2013).

[2] D. Seol, H. Taniguchi, J.-Y. Hwang, M. Itoh, H. Shin, S. W. Kim, and Y. Kim, Nanoscale **7**, 11561 (2015).

[3] W. P. Zhao, C. Shi, A. Stroppa, D. Di Sante, F. Cimpoesu, and W. Zhang, Inorg. Chem. **55**, 10337 (2016).

[4] J. B. Neaton, C. Ederer, U. V. Waghmare, N. A. Spaldin, and K. M. Rabe, Phys. Rev. B **71**, 014113 (2005).

[5] R. Seshadri and N. A. Hill, Chem. Mater. **13**, 2892 (2001).

[6] J. Park, B. G. Kim, S. Mori, and T. Oguchi, J. Solid State Chem. **235**, 68 (2016).

[7] H. Taniguchi, T. Nakane, T. Nagai, C. Moriyoshi, Y. Kuroiwa, A. Kuwabara, M. Mizumaki, K. Nitta, R. Okazaki, and I. Terasaki, J. Mater. Chem. C **4**, 3168 (2016).

[8] W. Cochran, Adv. Phys. **9**, 387 (1960).

[9] A. Girard, H. Taniguchi, S. M. Souliou, M. Stekiel, W. Morgenroth, A. Minelli, A. Kuwabara, A. Bosak, and B. Winkler, Phys. Rev. B **98**, 134102 (2018).

[10] K. Jin, Q. Wu, H. Geng, X. Li, L. Cai, and X. Zhou, High Press. Res. **31**, 560 (2011).

[11] C. Prescher and V. B. Prakapenka, High Press. Res. **35**, 223 (2015).

[12] V. Petricek, M. Dusek, and L. Palatinus, Z. Kristallogr. **229**, 345 (2014).

[13] A. Girard, T. Nguyen-Thanh, S. M. Souliou, M. Stekiel, W. Morgenroth, L. Paolasini, A. Minelli, D. Gambetti, B. Winkler, and A. Bosak, J. Synchrotron Radiat. **26**, 272 (2019).

[14] P. Hohenberg and W. Kohn, Phys. Rev. **136**, B864 (1964).

[15] J. P. Perdew, K. Burke, and M. Ernzerhof, Phys. Rev. Lett. **77**, 3865 (1996).

[16] S. J. Clark, M. D. Segall, C. J. Pickard, P. J. Hasnip, M. I. J. Probert, K. Refson, and M. C. Payne, Z. Kristallogr. **220**, 567 (2005).

[17] See Supplemental Material at http://link.aps.org/supplemental/10.1103/PhysRevB.99.064116 for tabulated values of lattice parameters under pressure.

[18] R. J. Angel, M. Alvaro, and J. Gonzalez-Platas, Z. Kristallogr. **229**, 405 (2014).

[19] A. Friedrich, B. Winkler, W. Morgenroth, J. Ruiz-Fuertes, M. Koch-Müller, D. Rhede, and V. Milman, Phys. Rev. B **90**, 094105 (2014).

[20] J. D. Jorgensen, J. Appl. Phys. **49**, 5473 (1978).

[21] U. Häussermann, P. Berastegui, S. Carlson, J. Haines, and J.-M. Léger, Angew. Chem., Int. Ed. Engl. **40**, 4624 (2001).

[22] A. Friedrich, E. A. Juarez-Arellano, E. Haussühl, R. Boehler, B. Winkler, L. Wiehl, W. Morgenroth, M. Burianek, and M. Mühlberg, Acta Crystallogr., Sect. B **66**, 323 (2010).

[23] L. F. Lundegaard, E. Makovicky, T. Boffa-Ballaran, and T. Balic-Zunic, Phys. Chem. Miner. **32**, 578 (2005).

[24] I. Efthimiopoulos, J. Kemichick, X. Zhou, S. V. Khare, D. Ikuta, and Y. Wang, J. Phys. Chem. A **118**, 1713 (2014).

[25] B. Winkler, V. Milman, and M. H. Lee, J. Chem. Phys. **108**, 5506 (1998).